Improved Quantum Sensing with a Single Solid-State Spin via Spin-to-Charge Conversion

J.-C. Jaskula, B.J. Shields, E. Bauch, M.D. Lukin, A.S. Trifonov, and R.L. Walsworth

Phys. Rev. Applied **11**, 064003 — Published 3 June 2019

DOI: 10.1103/PhysRevApplied.11.064003

Improved quantum sensing with a single solid-state spin via spin-to-charge conversion

J.-C. Jaskula,[1,2] B. J. Shields,[2,*] E. Bauch,[2] M. D. Lukin,[2] A. S. Trifonov,[1,2,3,†] and R. L. Walsworth[1,2,4]

[1] *Harvard-Smithsonian Center for Astrophysics, Cambridge, Massachusetts 02138, USA*
[2] *Department of Physics, Harvard University, Cambridge, Massachusetts 02138, USA*
[3] *Ioffe Physical-Technical Institute RAS, Saint Petersburg, Russia*
[4] *Center for Brain Science, Harvard University, Cambridge, Massachusetts 02138, USA*

Efficient optical readout of single, solid-state electronic spins at room temperature is a key challenge for nanoscale quantum sensing. Nitrogen-vacancy (NV) color centers in diamond have a fast optical spin-state readout mechanism, however it provides little information in a single shot, because the spin state is destroyed before many photons can be collected. Recently, a technique based on spin-to-charge conversion (SCC) has been demonstrated that circumvents this problem by converting the spin state to a long-lived charge state. Here, we study how the choice of spin readout technique impacts the performance of a single NV center in bulk diamond for quantum sensing applications. Specifically, we show that the SCC technique results in an order-of-magnitude improvement in spin readout noise per shot and a factor of five improvement in AC magnetometry sensitivity compared to the conventional optical readout method. Crucially, these improvements are obtained for a low collection efficiency, bulk diamond geometry, which opens up the SCC technique to a wide array of sensing applications. We identify applications where single shot spin readout noise, rather than sensitivity, is the limiting factor, e.g., low duty cycle pulsed sequences in biomagnetometry involving long deadtimes.

I. INTRODUCTION

Quantum defects in solids are emerging as the sensors of choice for detecting micrometer to nanometer phenomena in a wide range of systems in both the physical and life sciences. The Nitrogen-Vacancy (NV) color center in diamond is a prime example of such a solid-state spin defect, combining long-lived electronic spin coherence with the ability to prepare and read out the spin state optically [1]. For example, NV centers have been used for high-spatial resolution sensing of magnetic fields in cell biology [2], bioassays [3], neuroscience [4], nanoscale nuclear magnetic resonance (NMR) detection [5–7], and condensed matter physics [8–11]. An important figure of merit for this system is the spin readout noise per shot, specifying the accuracy with which the final state of the electron spin evolution can be measured in a single measurement attempt. Current room temperature NV experiments rely on a spin-dependent fluorescence signal that is restricted to a short detection window (∼250 ns), after which the spin is optically pumped into the $m_s = 0$ state, such that the spin-state-dependent fluorescence is typically limited to about a fraction of a photon per readout window for a single NV center [1]. Recently, a new NV spin readout technique based on spin-to-charge conversion (SCC) that overcomes this limitation was demonstrated in diamond nanobeams [12], in which the single NV fluorescence is enhanced by an order of magnitude compared to NV centers in bulk diamond. A similar protocol has also been demonstrated using high-intensity, near-infrared laser pulses and single NV centers under solid immersion lenses to achieve a spin-to-charge mapping via selective ionization of the singlet manifold [13]. The key point of the latter techniques is the use of a long charge state readout that exhibits a high fidelity as a result of a strong integrated optical signal. However, since quantum sensors destroy the final state after readout, the question of which readout technique delivers the best sensing performance is closely related to the number of repetitions of the pulse sequence and hence depends on the timescale of the probed phenomenon, as well as the duration and efficiency of the spin readout. Thus, even though the SCC technique reads the NV quantum state out more efficiently than conventional spin-dependent fluorescence, the length of the readout gate could still be a limitation in the case of short NV spin coherence times. Here we investigate the advantages and drawbacks of the use of both SSC and conventional NV spin readout in the context of quantum sensing. We also highlight which readout protocol is favored depending on the intended application.

Our study is further motivated by the fact that the SCC technique requires longer readout gates with NV centers in bulk diamond than with nanobeams, due to the lower collection efficiency of the former. Consequently, it does not necessarily outperform conventional fluorescence spin readout. In particular, SCC readout fidelity can be improved with lower excitation powers and longer readout gates, only up to the point that detector noise becomes significant. Experimentally, we find that in bulk diamond SCC readout can provide an order of magnitude improvement in single NV spin readout noise per shot. We then assess the performance of single NV quantum sensors using both SCC and conventional readout for two common sensing regimes. In the case of sinusoidal (AC) uninterrupted magnetic field signals, we compare the sensitivity, which characterizes how precisely one can mea-

* Present address: Department of Physics, Basel University, Basel, Switzerland.
† Deceased

sure a weak magnetic field during a finite amount of time (e.g., one second). We demonstrate an improvement in single NV AC magnetometry sensitivity of about a factor of five using SCC readout, relative to conventional readout. In contrast, sensitivity is not the optimal figure of merit for many applications such as sensing on-demand pulsed fields. In this case, the single shot precision – equivalent to the smallest signal that can be detected in a single measurement independent of the time it takes – is a better figure of merit. In this case, we again find that SCC readout outperforms conventional readout for single NV quantum sensing protocols like "coherently averaged synchronized readout" (CASR) where the sequence is triggered by an external clock or coherent signal [14–16]. To overcome the limitations of finite NV spin lifetime while maintaining high spectral resolution sensing, the CASR protocol typically includes time fillers that can extend the duration of the NV readout and thereby make SCC especially advantageous.

II. SPIN READOUT PROTOCOLS

A. Spin-dependent fluorescence

The conventional mechanism for room temperature optical readout of the NV electron spin (S = 1 for NV^- charge state) is based on a spin-dependent intersystem crossing from the optical excited state into a manifold of optically dark singlet states. Under excitation with 532nm light, an NV center initially in $m_s = 1$ (or $m_s = -1$) is shelved into the metastable singlet level with about a 50% probability [17] and remains dark under subsequent excitation during the singlet state lifetime followed by preferential decay to the $m_s = 0$ state; whereas an NV center initially in $m_s = 0$ will continue to cycle and scatter photons during this readout time. These spin-state-dependent pathways induce repolarization of the NV spin to the $m_s = 0$ ground state and constrain the detection window duration to ∼250 ns at room temperature. In practice, even with high-NA optics and index-matching techniques, the fluorescence collected from a single NV center in bulk diamond is limited to about $n \approx 0.022$ photons per readout with a low spin-state contrast of typically $V \approx 25\%$ (Fig. 1(a)) [18]. Thus, effective readout of the NV spin state can only be achieved statistically after many averages. Standard approaches to overcome this limitation involve using macroscopic ensembles of NVs [19–21] or diamond nanostructures [22–24], in order to boost the fluorescence signal from the NV centers. Such techniques have their limitations, namely reduced spatial resolution and coherence time in the case of ensemble measurements, or limited sensing area and scalability in the case of photonic nanostructures. Therefore, techniques for improved readout of single NV centers in bulk diamond are of great interest.

A complementary approach is to develop readout techniques that transfer the spin state to more robust degrees of freedom than the relatively short-lived singlet. One such technique involves the transfer of spin information to the NV nuclear spin, which can subsequently be repetitively read out multiple times through the NV electronic spin [25]. This technique is capable of approaching the spin-projection noise limit, but has the disadvantage of requiring strong magnetic fields as it is limited by the field-dependent depolarization time of the NV nuclear spin.

B. Spin-to-charge state conversion

Spin-to-charge conversion (SCC) readout [12] transfers the spin state to the charge state of the NV, followed by a high-fidelity charge state measurement. This method has the advantage of being able to reach spin readout noise levels as low as twice the spin projection noise level, while being fully optical and easily incorporated in a confocal microscope, potentially with ensembles of NV centers.

NV centers are found mainly in two charge configurations [26], NV^0 and NV^- (Fig. 1(b)), which can be switched via a photo-ionization process [27]. The NV^- spin state (S = 1) can be optically initialized and is used for quantum sensing; the NV^0 spin state (S = 1/2) cannot be optically initialized. However, the NV center charge state can be read out in a single shot with a laser beam at 594nm, which efficiently excites NV^- but only weakly NV^0, producing a high fluorescence contrast between the two charge states [28–30] (Fig. 1(c)). For high readout fidelity, photo-ionization must be suppressed during readout, requiring low laser powers (as low as a few microwatts) and long readout times (from tens of microseconds to few milliseconds, depending on the desired single shot charge state readout fidelity). To switch between the charge states, a green laser beam (532 nm) initializes the charge state of the NV center preferentially to NV^- with 70% probability; while a 10-nanosecond pulse of red light (637 nm) almost ideally ionizes the NV center from NV^- to NV^0 via a two-step process that occurs between the NV center ground state and the conduction band.

The ionization process under 637nm illumination can be made spin-state-dependent by first shelving one spin state into the metastable singlet level, for which ionization is suppressed. In particular, the $m_s = 1$ population can be protected from ionization by first transferring it via a 594nm, 50ns-long pulse into the singlet state, before ionizing the remaining triplet state population (mainly $m_s = 0$) with an intense 637nm pulse. The 637nm light does not excite the singlet state, so the ionization process is blocked for $m_s = 1$, and the NV remains in the negative charge state. We implement this spin-to-charge conversion with the sequence depicted in Figure 1(d). We plot the photon number distributions in Figure 1(e) for the two cases where the NV center is prepared in $m_s = 0$ (no microwave pulse) and $m_s = 1$ (microwave π pulse), illustrating the SCC efficiency. As expected, $m_s = 0$ is converted almost entirely to NV^0, while $m_s = 1$ re-

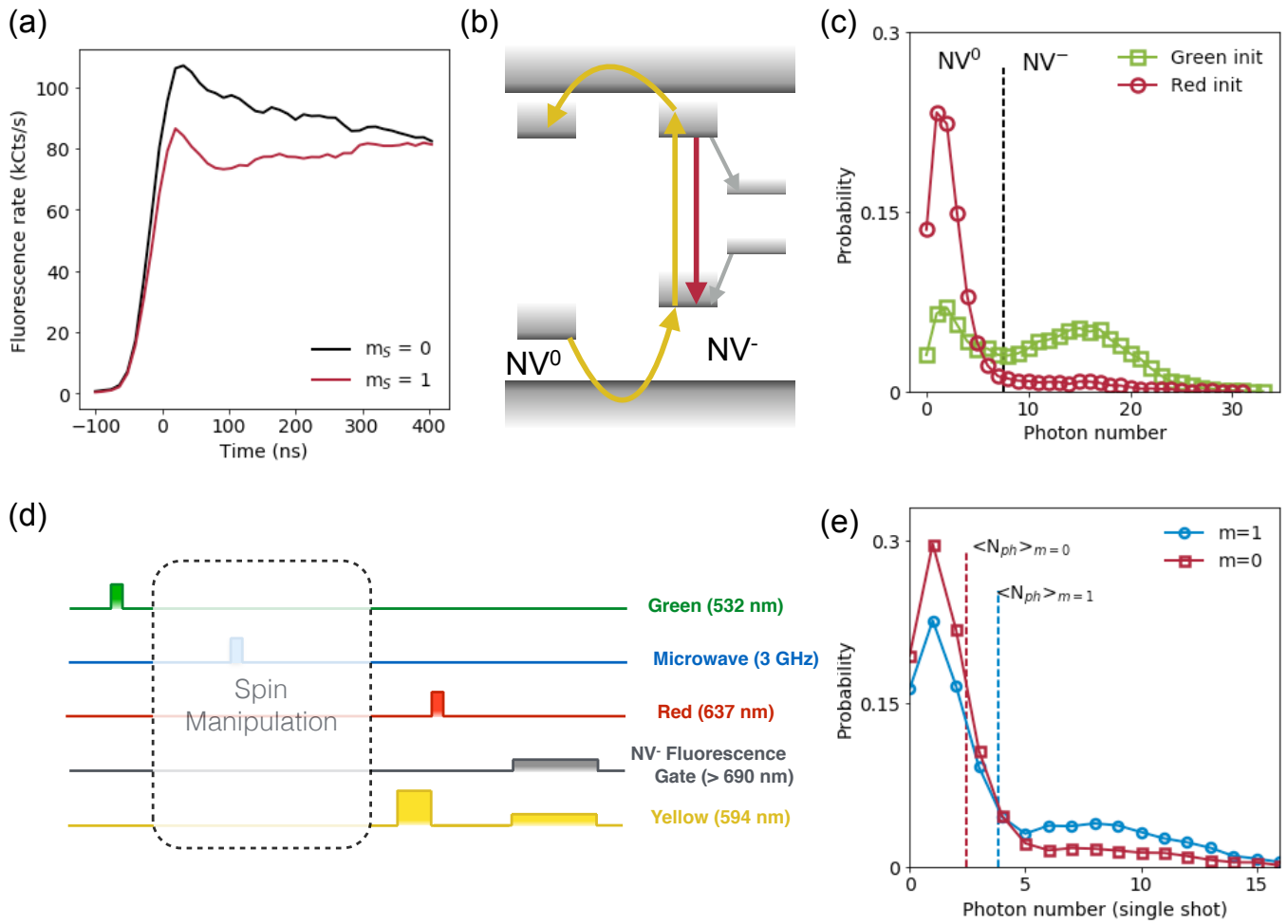

FIG. 1. (a) Example of spin-state-dependent transients in the fluorescence of a single NV center in bulk diamond, allowing for spin readout. (b) Energy levels of the neutral and negatively charged NV center. The NV^- electron spin can be polarized via decays through singlet states. A yellow (594 nm) laser beam only excites NV^-, leaving NV^0 dark, but it can also ionize NV^- to NV^0 (and induce recombination from NV^0 to NV^-). However, these processes are suppressed at low power, enabling high fidelity charge state readout. (c) Initialization of the charge state can be done with a green (532 nm) laser beam to prepare the negative charge state with a 70% probability. A red beam (637 nm) efficiently ionizes the NV center from NV^- to NV^0. (d) General sequence for NV quantum sensing. (e) Example measured photon number distribution shows the efficiency of the spin-to-charge conversion (SCC) technique for a single NV center in bulk diamond. The dashed lines indicate the mean values of each distribution and show a spin readout contrast of 36%.

mains in NV^- to a large degree. From the mean values of the two distributions ($\langle N_{\rm ph}\rangle_{\rm m=0} = 2.4(2)$ and $\langle N_{\rm ph}\rangle_{\rm m=1} = 3.8(3)$), we extract a spin-state contrast of 36(1)%, which is larger than for the conventional (singlet-state) readout scheme (by about a factor of 1.5x) due to the fact that the ionization occurs when the population of the singlet state is maximum. More importantly, the robustness of the charge states allows for the collection of a relatively large number of photons in a single shot (about 5 photons in a 1 ms time window experimentally). This increased photon number largely reduces the contribution of photon shot noise in the measurement, leaving only spin-projection noise and conversion noise during the spin-to-charge mapping. However, we note that the photon shot noise suppression has a lower bound given by detector dark counts (200 ph/s in our case). This prevents us from using very low readout powers, which places a limit on our achievable charge readout fidelity.

We define the spin readout noise per shot σ_R as the ratio between the measured spin noise and the spin projection noise $\sigma_{\rm SPN} = \sqrt{p_0(1-p_0)}$, where p_0 is the probability of detecting one projection, e.g., $m_s = 0$, of our effective two-level spin system. The spin readout noise can be estimated directly from the collected photon distribution for each class of spin. In the case of SCC readout, a perfect mapping would link the spin state $m_s = 0$ and $m_s = 1$ to the neutral charge state NV^0 and negatively charged state NV^-, respectively. We define errors

ϵ_0 and ϵ_1 to be the probabilities that the detected charge state deviates from such a perfect mapping. Then we can recast the spin readout noise per shot expressed in [12] as $\sigma_R = \sqrt{1-(\epsilon_0-\epsilon_1)^2}/(1-(\epsilon_0+\epsilon_1))$. These errors can be straightforwardly estimated from Figure 1(e) by choosing a threshold (here equal to 5 photons) that distinguishes the charge states from each other as depicted in Figure 1(c). In the experiments reported here, we obtain $\epsilon_0 = 0.14(3)$ and $\epsilon_1 = 0.69(4)$, which results in $\sigma_R = 4.9(1.4)$. For comparison, conventional NV spin-state readout is limited by photon shot noise [1, 12]. The spin readout noise per shot consequently becomes $\sigma_R \simeq 2(V\sqrt{n})^{-1} \approx 54$ for single NV confocal detection with n and V as previously defined (Fig. 1(a)). We measured the SCC readout efficiency for 19 NV centers in bulk diamond sample A (see Appendix A) and found no significant difference between the NVs in the spin readout noise per shot, with a measured standard deviation $\Delta\sigma_R \approx 0.7$. The following results in Figs. 1-6 are thus from measurements on the same single NV center in sample A.

III. APPLICATION TO MAGNETIC SENSING

As a proof of concept of the performance of the SCC method for quantum sensing, we use a single NV center in diamond sample A as a nanoscale AC magnetic field sensor. Oscillating magnetic fields can be probed by applying a synchronized Hahn-echo sequence. During a sensing period τ, the NV center's quantum state evolves under the influence of the AC magnetic field as well as environmental noise. This evolution is manifested by a phase accumulation that is converted into an optically-readable spin state population difference, either by SCC or conventional readout. Because of the noise environment, such phase accumulation is limited to the characteristic coherence time T_2. For a single NV, T_2 can approach one millisecond at room temperature [31, 32] via the implementation of dynamical decoupling sequences that act as filter functions to suppress the effects of noise fluctuations. In our experiment, we drive the NV center's electronic spin into a superposition of $m_s = 0$ and $m_s = 1$ that acquires a relative phase scaling linearly with the applied AC magnetic field amplitude $\phi = \frac{2\mu_B}{\pi\hbar} B\tau = \alpha B\tau$ [33, 34]. Here we use a 100-turn coil to create an external arbitrary AC field that is aligned along the NV axis to within a few degrees and applied only during the Hahn-echo sequence. Because of the low field's frequency ($\sim$ 1 kHz) and amplitude ($\sim$ 100 nT), its perpendicular component does not affect the evolution and control of the NV spin. The measurement protocol results in a rotation of the Bloch vector in the equatorial plane, which is observed as a sinusoidal oscillation of the NV fluorescence or SCC signal with AC magnetic field amplitude, as the phase is transferred to a population difference (Fig. 2(a)). For the same total acquisition time, the residual plot in the bottom of Figure 2(a) demonstrates that SCC readout provides better sensitivity to the AC field amplitude than conventional readout.

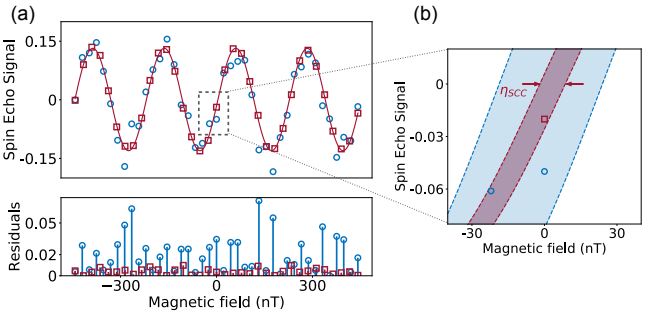

FIG. 2. (a) Examples of measured normalized single NV fluorescence signals as a function of AC field magnitude using a Hahn-echo sequence with conventional (blue) and SCC (red) readout techniques. The interrogation time τ is 236.52 μs and matches the inverse of the AC magnetic field frequency of about 4.2 kHz. Each data point is averaged for two minutes, showing improved sensitivity for the SCC scheme, as indicated by reduced residuals. (b) Zoom showing the improved sensitivity, from 45(12) nT/$\sqrt{\text{Hz}}$ for conventional readout to 9(1) nT/$\sqrt{\text{Hz}}$ for the SCC technique, at the most sensitive operating point (around zero AC magnetic field amplitude).

Figure 2(b) is a zoom around the point of zero AC magnetic field amplitude, where the NV magnetometer sensitivity $\eta(\tau)$ is optimal, which we estimate by [1]:

$$\eta(\tau) = \sigma_R \frac{e^{\left(\frac{\tau}{T_2}\right)^p}}{\alpha\sqrt{\tau}} \sqrt{\frac{t_{\text{init}} + \tau + t_{\text{ro}}}{\tau}}. \quad (1)$$

Here, α is the scaling factor between the phase acquired and the field amplitude measured, and p is an exponent containing information related to the spin bath [35]. $\sqrt{(t_{\text{init}} + \tau + t_{\text{ro}})/\tau}$ is a time penalty, where the initialization time and the readout time are denoted respectively t_{init} and t_{ro}. Experimentally, the sensitivity can be quantified from statistical measurements of the fluorescence signal. In figure 2(a), each data point is the average value of a large dataset containing the results of all realizations of the pulse sequence at a particular field strength. These datasets can be subdivided into M realizations of total acquisition time T, from which we extract a standard deviation $\sigma_f(T)$. This is then translated into magnetic field units as $\eta = \sigma_f(T)\sqrt{T}/dS$, where dS is the slope of the Hahn-echo signal taken at the point of zero AC magnetic field amplitude (Figure 2(b) and Appendix C). For our demonstration experiment, we find an improvement of a factor 5 in AC magnetic field sensitivity for the SCC method, 9(1) nT/$\sqrt{\text{Hz}}$, relative to conventional readout, 45(12) nT/$\sqrt{\text{Hz}}$.

We next investigate the dependence of this sensitivity improvement on the evolution time τ. Increasing this time results in more phase accumulation, i.e., faster oscillations of the magnetometry curve in Figure 2(a), which

is only favorable up to the point where spin decoherence reduces the measurement contrast. We repeat the analysis previously done in Figure 2 for different interrogation times of the Hahn-echo sequence ranging from 26 μs to 680 μs. The frequency of the applied field is adapted to match the length of the microwave sequence $\nu_{\mathrm{AC}} = 1/\tau$. We report in Figure 3 the measured sensitivities with conventional and SCC readout, where the durations were fixed to $t_{\mathrm{init}} = 30$ μs for the initialization pulse, $t_{\mathrm{ro}} = 3$ μs for the conventional readout pulse, and $t_{\mathrm{ro}} = 350$ μs for the SCC readout. According to equation (1), there is an optimum of sensitivity at $\tau = T_2/2 = 232$ μs for conventional readout (for which the initialization and readout time are negligible and p $\approx$ 1), as is clearly visible in Figure 3. The SCC technique performs noticeably better than conventional readout over a wide range of evolution times between 26 μs to 680 μs. As τ increases and becomes significantly longer than the readout time, the relative performance gain approaches its maximum value, $\sigma_R^{\mathrm{conven.}}/\sigma_R^{\mathrm{SCC}} \leq 10$. At the other extreme, we expect that conventional readout will provide better sensitivity when τ is short, since short spin readout times allow for fast repetition of quantum sensing sequences. We find that this regime is not reached yet at evolution times as short as 26 μs, where the sensitivity improvement is still in favor of the SCC technique by a factor of two (Fig. 3). Moreover, we note that in this case of high frequency AC magnetic fields, dynamical decoupling sequences are useful tools that benefit greatly from SCC readout because they both move the filter function's central frequency to match the field frequency, and significantly extend the coherence time of the NV sensor. From the parameters of each fit given by equation (1), we determine that the spin readout noise per shot σ_R for conventional readout is $\sigma_R^{\mathrm{conven.}} = 60(7)$ and $\sigma_R^{\mathrm{SCC}} = 5.0(7)$ for SCC readout, confirming the values reported above. Interestingly, the fitted p parameter in (1) is different for the two readouts ($p_{\mathrm{SCC}} = 1.0(3)$ and $p_{\mathrm{conven.}} = 1.3(2)$), possibly because the spin bath dynamics is affected under laser illumination of different wavelengths, so that the sensitivity improvement is not yet saturated for long ($\geq$ 680 μs) evolution time.

Since the time penalty term in (1) becomes significant only for a readout time comparable to or longer than the interrogation time, the SCC sensitivity improvement can be optimized for long interrogation times by increasing the readout time (and consequently decreasing σ_R). We now fix the evolution time of $\tau = 236.52$ μs, corresponding to a frequency of about 4.2 kHz for the AC signal field. We search for the optimal operating point by varying the readout duration t_{ro} and plotting the corresponding sensitivities in Figure 4(a). We show the best sensitivity for SCC readout is 9(1) nT/$\sqrt{\mathrm{Hz}}$ for $t_{\mathrm{ro}} = 100$ μs.

In practice, the duty cycle of quantum sensors can also be limited by external parameters, e.g., the repetition rate of the recorded events. In such scenarios, the correct figure of merit is the single shot precision. In particular, one can take full benefit of long readout time windows of a few milliseconds to improve the performance of the spin readout and consequently of NV magnetometers using the SCC technique. For example, as shown in Figure 4(b), we report an AC magnetic field amplitude uncertainty of 307(29) nT in a single SCC measurement with a 5 ms readout time, for which the photon shot noise is nearly totally suppressed. This uncertainty is an order of magnitude smaller than with conventional NV spin readout.

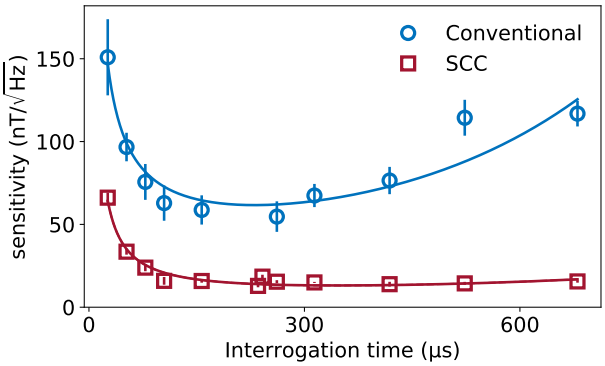

FIG. 3. Measured single NV AC magnetic field sensitivity as a function of interrogation time. Solid lines are fits using Eq. (1) fixing $T_2 = 461.5$ μs, $t_{\mathrm{init}} = 30$ μs, and $t_{\mathrm{ro}} = 350$ μs (3 μs) for SCC (conventional) readout, as independently measured. The SCC scheme is even more advantageous than the conventional readout technique at long interrogation time, where single, efficient readouts are superior to multiple repetitions of the readout protocol.

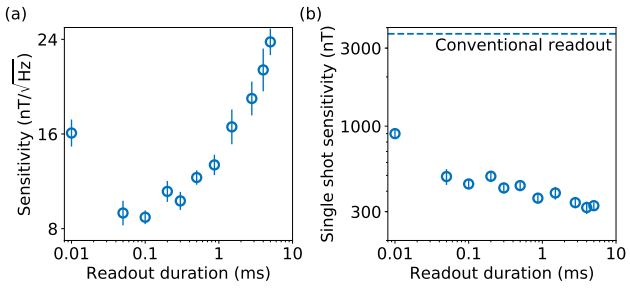

FIG. 4. (a) Optimization of the SCC technique's AC magnetic field sensitivity (about 4.2 kHz signal field) by tuning the readout duration to limit the inactive time. Here we adapt the readout power for each readout duration to maximize the charge state readout fidelity. (b) Smallest AC magnetic field amplitude measurable with the SCC technique (i.e., with a signal-to-noise ratio of 1) for a single realization of the magnetometry sequence, again with a signal field frequency of about 4.2 kHz.

IV. CONCLUSION

In this manuscript, we compared two spin readout techniques for quantum sensing with single NV centers in bulk diamond. Specifically, we find that spin-to-charge conversion (SCC) provides a significant improvement in both spin readout noise per shot and AC magnetometry sensitivity compared to the conventional method of spin-state-dependent fluorescence. We expect that SCC readout will also be beneficial for any quantum sensing protocol that benefits from a long qubit coherence time, such as T_2-limited thermometry [36] or ancilla-assisted DC magnetometry [37]. Furthermore, for typical NV spin dephasing times observed in isotopically purified ^{12}C samples with low Nitrogen concentration ($T_2^* \approx 50$ μs) [38], SCC readout should be applicable to Ramsey-like DC magnetometry with a two-fold sensitivity improvement.

Our work focuses on NV centers in bulk diamond, for which we typically detect around 100 kphotons/s at saturation. When using a low-intensity yellow laser, we find that the fluorescence rate approaches the lower bound given by technical noise, where the charge state readout fidelity is significantly reduced. In these conditions, shallow NV centers, which display shorter coherence times and lower fluorescence rates than typical isolated bulk NV centers, might not be able to exploit fully the potential of the SCC technique. Nonetheless, we report in Appendix E that charge state readout of a shallow (~ 3 nm) NV center is feasible, paving the way for use of the SCC technique with quantum sensors near the diamond surface. Similar success in applying the SCC technique to shallow NV centers has recently been reported in [39].

Moreover, SCC readout is well suited to pulsed measurement protocols, for which it is not necessary to optimize the duty cycle of the sensor; and hence one can take advantage of dead time to increase the fidelity of the readout. One such technique is coherently averaged synchronized readout (CASR) [14–16]. By synchronizing an entire sensing sequence to a coherent, long-lived signal of interest, one can improve the spectral resolution of a spin-based sensor such as an NV beyond the limit given by the spin coherence and polarization times (T2 and T1) [16]. This CASR technique provides, e.g., Hz-scale spectral resolution for NV measurements, enabling NMR chemical shifts and scalar couplings to be measured in picoliter samples [16]. Thus, to assure good synchronization over many NV readouts, CASR inserts regular waiting times in the pulse sequence. The SCC technique can benefit from these deadtimes to perform longer and more efficient readout of the NV center's spin state. A second SCC application is the detection of pulsed magnetic fields with low repetition rates, e.g., those created by neuron action potentials with typical pulse timescales of milliseconds and delays between pulses of 10-100 milliseconds [4]. In such cases, SCC sensitivity is expected to improve by an order of magnitude compared to conventional readout, down to $\sim$300 nT for a single realization of the experimental protocol. Finally, because the neutral charge state is a dark state, SCC readout is also well suited for NV ensemble measurements [40, 41] and superresolution techniques [42, 43], which both suffer from background fluorescence. Indeed, off-axis NV centers are not affected by the microwave pulses and are consequently ionized during the spin to charge mapping.

ACKNOWLEDGMENTS

This material is based upon work supported by, or in part by, the U. S. Army Research Laboratory and the U. S. Army Research Office under contract/grant number W911NF1510548, the DARPA Quantum Assisted Sensing And Readout (QuASAR) program (contract #HR0011-11-C-0073), the CUA, the Gordon and Betty Moore Foundation, the Vannevar Bush Fellowship, and the NSF EPMD, PoLS, and INSPIRE programs.

APPENDIX

A. Diamond samples

We used two diamond samples for this study. Sample A is a CVD diamond with [NV] $\sim$ 0.2 ppb, [N] $\sim$ 0.1 ppm, and a natural abundance of 13C nuclear spins. A single NV in Sample A was used for all the quantitative results presented in Figs. 1-6. Sample A was also used for the characterization of SCC readout efficiency for 19 NV centers.

Sample B has an epitaxially grown, 99.99% ^{12}C layer, which was left unpolished. An implantation mask was made on top of the ^{12}C layer prior to implanting ^{14}N ions at 2.5 keV, with a resulting estimated average depth in the diamond of 3 nm. The sample was annealed for 8 hr at 900 °C. We prepared 12 regions of 50 μm-diameter with densities of implanted nitrogen gradually varying from about 10^9 cm^{-2} to 10^{12} cm^{-2}. A single NV in Sample B was studied in the region of highest N density: this NV showed qualitatively similar charge state dynamics to the single NVs in bulk diamond in Sample A; see Fig. 7.

B. Experimental apparatus

The experimental setup is a confocal microscope adapted for NV spin-state measurements via both the SCC and conventional fluorescence techniques. Three laser beams (at 532, 594, and 637 nm) are coupled into single mode optical fibers to improve their spatial mode, and are then combined together with dichroic mirrors. A DPSS laser is used together with an acousto-optic modulator (AOM) to generate the green (532 nm) laser pulse. The shelving yellow (594 nm) laser pulse and charge readout are both made with the same laser (HeNe

1.5mW) and AOM. To switch quickly from a relatively high yellow laser power (500 μW) for the protective step to a low power (5 μW) for the charge-state readout, two RF control signals are generated with voltage-controlled oscillators and controlled with RF switches. The red (637 nm) ionizing optical pulses are generated with a diode laser (HL63133DG, Thorlabs, 170 mW CW at 637 nm). The optical pulses are controlled with a pulse generator (AVO-2L-C-GL2, Avtech, 500 ps rise time, 2A), resulting in square pulse widths between 4 and 30 ns. The three laser beams are focused on a single NV in bulk diamond with a 1.45 NA, oil-immersion objective. The NV fluorescence (∼90 kcounts/s) is collected through the same objective and then detected with an avalanche photodiode. A 150 μm pinhole restricts the longitudinal point-spread function to 500 nm and avoids out-of-focus background fluorescence from other NV centers.

C. Coherence time measurement

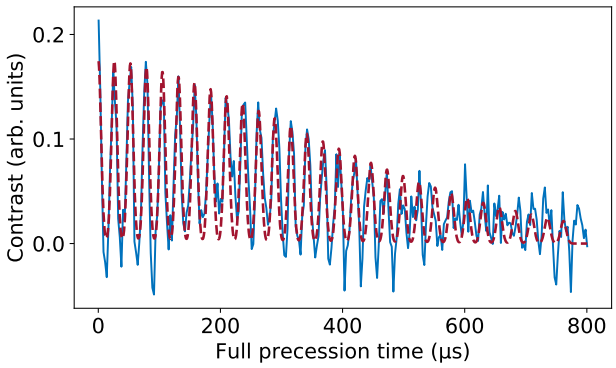

FIG. 5. Coherence decay of a single NV center in sample A measured with a Hahn-echo sequence. We plot the fluorescence signal S in solid blue. Interactions with the ^{13}C nuclear spin bath cause collapses and revivals. The Hahn-echo signal envelope is fitted with an exponential decay function modulated by a sum of Gaussian functions centered at multiples of the Larmor precession time (dashed red line).

In the absence of an applied AC magnetic field, the single NV coherence time T_2 can be measured using the same Hahn-echo sequence as described in the main text. Experimentally, we interleave two different Hahn-echo pulse sequences: (i) the last $\pi/2$ pulse of the first sequence is applied along an arbitrary axis X; while (ii) the same pulse of the second sequence is applied along the opposite axis -X. This protocol projects the spin population either on (i) $m_s = 0$ or (ii) $m_s = 1$, delivering a fluorescence signal F_0 (resp. F_1). The plotted signal in Figures 2(a) and 5 are the following linear combination of F_0 and F_1: $S = (F_0 - F_1)/(F_0+F_1)$. As we vary the free evolution time τ, we find that the superposition of $m_s = 0$ and 1 decays to an incoherent state in a time $T_2 = 461.5$ μs. Due to the presence in sample A of ^{13}C atoms in the diamond lattice (at the natural abundance of 1.1%), the coherence of the NV center is modulated by revivals that occur at multiples of the Larmor precession time $t_{rev} = 26.28$ μs. AC magnetometry can only be done at evolution times that corresponds to the different revivals. Consequently, the optimal experimental sensitivity is achieved for $\tau_{opt} = 236.52$ μs $\simeq T_2/2$.

D. Charge state initialization via post-selection

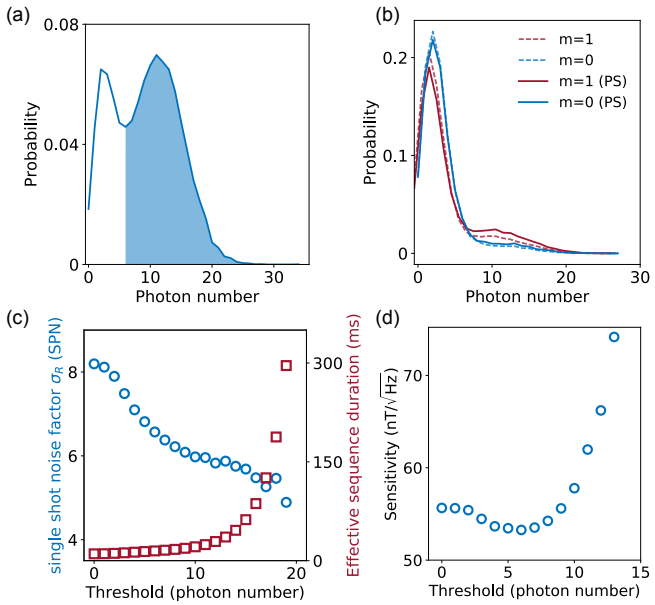

FIG. 6. Post-selection enhancement of SCC technique. (a) Photon distribution recorded in an initial charge readout pulse prior to microwave manipulation. The distribution of all sequences (solid line) shows that a significant fraction of events is executed on the neutral charge state and can be discarded to keep mainly results obtained with NV^- (filled area). (b) Photon distributions after post-selecting for NV^- (solid lines) have greater distinguishability than the distributions for all events (dashed lines). The Kolmogorov–Smirnov test gives a distinguishability of 0.12 against 0.08 for no post-selection. (c) Spin readout noise per shot as a function of threshold, and effective sequence time. Eliminating initial NV^0 events improves the efficiency of SCC mapping at the cost of increasing the sequence duration. (d) AC magnetic field sensitivity (about 4.2 kHz signal field) for different thresholds, showing a 5% improvement in sensitivity by post-selecting for the initial NV charge state. The length of both charge-state readout windows (20 ms in total) limits the absolute sensitivity to 53(16) nT/$\sqrt{\text{Hz}}$. Alternatively, very short time windows that would allow for the detection a single photon would be enough to determine the charge state of the NV center.

The 30 μs-long green initialization leaves the NV center

in its neutral charge state one third of the time, allowing for a substantial improvement in the SCC technique performance by detecting aberrant initializations prior to the coherent microwave manipulation. This protocol can be performed with charge-state readout capability with either a 'try till success' polarization technique or by post-selecting on the initial charge state being NV^-. Although the former offers the best sensitivity, it also requires fast readout electronics to compute the result of the first charge state readout. As a proof-of-concept, we implemented the latter by reading out the charge state of the NV center with a 10 ms long yellow readout pulse. The ionization has a quadratic behavior with respect to the excitation power, while it is linear for the fluorescence. So it is realistic to suppress ionization processes during the charge verification step. In practice, charge state jumps are still being observed with 10ms-long readout gates and an accordingly-chosen excitation power. Indeed, from subsequent measurements of the charge state, we estimate that the probability of ionizing the NV center after detecting it in the good charge state NV^- is about 10%. This leads to an increase of the initial spin readout noise per shot to about 8 in Figure 6 (from about 7 due to non optimized experimental parameters). In Figure 6(a), we plot the distribution of photons obtained from the first readout gate (blue curve). The post-selection is conditioned on having acquired a number of photons during the first charge state readout pulse that is strictly higher than a certain threshold (6 photons in Figure 6(a), filled blue area). Because we mainly reject sequences where the NV center is in NV^0, the distinguishability between the spin states is enhanced (Fig. 6(b)). To further demonstrate the improvement due to post-selection, we measure the readout noise for various thresholds. We see in Figure 6(c) that σ_R decreases faster at low threshold because we remove measurements where the NV center could not be used to sense any magnetic fields. After a threshold that corresponds to the visual limit between NV^0 and NV^-, the slope becomes less pronounced as we discard good measurements. In parallel, we estimate the cost of rejecting measurements by computing an effective sequence time. The AC magnetic field sensitivity can be improved if σ_R decreases faster than the square root of the effective sequence time increases (eq. (1)). We show that this is indeed the case for thresholds smaller than 6 photons per readout pulse, with an improvement of about 5% (Fig. 6(d)). Because of a technical limitation, the second charge state readout had to be of the same length as the first, which is the main limitation to the absolute value of the sensitivity.

E. Charge state readout of shallow NV centers

Shallow implanted NV centers are a promising modality for nanoscale magnetic resonance imaging and single molecule detection due to the strong dipolar and hyperfine interactions with electronic and nuclear spin species located on the diamond surface [44–46]. Adversely, surface effects tend to shorten the coherence time of shallow NVs, typically to tens of microseconds, and could also potentially modify their charge state dynamics. We show in Figure 7 that we see no change in the charge state dynamics of shallow NV centers; and also that they can still be read out via SCC with high fidelity. We plot in Figure 7(a) a typical time trace of the observed fluorescence, under constant 594nm light illumination, from a single NV center implanted 3 nm below the surface (measured by a nanoscale NMR technique [47]) exhibiting the expected behaviour: i.e., ionization and recombination between charge state NV^0 (low fluorescence level) and NV^- (high fluorescence level).

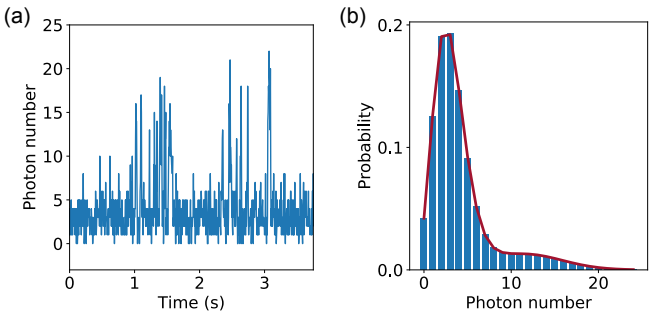

FIG. 7. (a) An example of time traces of a shallow ($\sim$ 3 nm deep) NV center's fluorescence under 594nm light illumination, revealing charge state jumps. (b) Photon number distribution displaying two levels of fluorescence. The red line is a numerical fit based on the master equation that describes the behaviour of the charge state under a 594nm light illumination [12].

The histogram of such time traces is plotted in Figure 7(b) and displays two peaks associated with these two levels of fluorescence. We perform a numerical fit based on the master equation that describes the behaviour of the charge state under a 594nm light illumination [12] and extract the fluorescence rates $\gamma_0 = 200$ Hz and $\gamma_- = 1.3$ kHz, the ionization rate $g_0 = 45$ Hz, and the recombination rate $g_- = 6$ Hz for an excitation power of 280 μW. These rates are very similar to those measured with NV centers in bulk diamond and indicate that SCC readout can provide a similar improvement with shallow NV centers as that reported in the main text for deep NVs.

[1] J. M. Taylor, P. Cappellaro, L. Childress, L. Jiang, D. Budker, P. R. Hemmer, A. Yacoby, R. Walsworth, and M. D. Lukin, High-sensitivity diamond magnetome-

ter with nanoscale resolution, Nat. Phys. **4**, 810 (2008).
[2] D. Le Sage, K. Arai, D. R. Glenn, S. J. DeVience, L. M. Pham, L. Rahn-Lee, M. D. Lukin, A. Yacoby, A. Komeili, and R. L. Walsworth, Optical magnetic imaging of living cells, Nature **496**, 486 (2013).
[3] D. R. Glenn, K. Lee, H. Park, R. Weissleder, A. Yacoby, M. D. Lukin, H. Lee, R. L. Walsworth, and C. B. Connolly, Single-cell magnetic imaging using a quantum diamond microscope, Nat. Methods **12**, 736 (2015).
[4] J. F. Barry, M. J. Turner, J. M. Schloss, D. R. Glenn, Y. Song, M. D. Lukin, H. Park, and R. L. Walsworth, Optical magnetic detection of single-neuron action potentials using quantum defects in diamond, Proc. Natl Acad. Sci. USA **113**, 14133 (2016).
[5] S. J. DeVience, L. M. Pham, I. Lovchinsky, A. O. Sushkov, N. Bar-Gill, C. Belthangady, F. Casola, M. Corbett, H. Zhang, M. Lukin, H. Park, A. Yacoby, and R. L. Walsworth, Nanoscale NMR spectroscopy and imaging of multiple nuclear species, Nat. Nanotech. **10**, 129 (2015).
[6] I. Lovchinsky, A. O. Sushkov, E. Urbach, N. P. de Leon, S. Choi, K. De Greve, R. Evans, R. Gertner, E. Bersin, C. Müller, L. McGuinness, F. Jelezko, R. L. Walsworth, H. Park, and M. D. Lukin, Nuclear magnetic resonance detection and spectroscopy of single proteins using quantum logic, Science **351**, 836 (2016).
[7] A. O. Sushkov, I. Lovchinsky, N. Chisholm, R. L. Walsworth, H. Park, and M. D. Lukin, Magnetic resonance detection of individual proton spins using quantum reporters, Phys. Rev. Lett. **113**, 197601 (2014).
[8] J.-P. Tetienne, T. Hingant, J.-V. Kim, L. H. Diez, J.-P. Adam, K. Garcia, J.-F. Roch, S. Rohart, A. Thiaville, D. Ravelosona, and V. Jacques, Nanoscale imaging and control of domain-wall hopping with a nitrogen-vacancy center microscope, Science **344**, 1366 (2014).
[9] S. Kolkowitz, A. Safira, A. A. High, R. C. Devlin, S. Choi, Q. P. Unterreithmeier, D. Patterson, A. S. Zibrov, V. E. Manucharyan, H. Park, and M. D. Lukin, Probing Johnson noise and ballistic transport in normal metals with a single-spin qubit, Science **347**, 1129 (2015).
[10] T. van der Sar, F. Casola, R. Walsworth, and A. Yacoby, Nanometre-scale probing of spin waves using single-electron spins, Nat. Commun. **6**, 7886 (2015).
[11] M. Pelliccione, A. Jenkins, P. Ovartchaiyapong, C. Reetz, E. Emmanouilidou, N. Ni, and A. C. Bleszynski Jayich, Scanned probe imaging of nanoscale magnetism at cryogenic temperatures with a single-spin quantum sensor, Nat. Nanotech. **11**, 700 (2016).
[12] B. J. Shields, Q. P. Unterreithmeier, N. P. de Leon, H. Park, and M. D. Lukin, Efficient readout of a single spin state in diamond via spin-to-charge conversion, Phys. Rev. Lett. **114**, 136402 (2015).
[13] D. A. Hopper, R. R. Grote, A. L. Exarhos, and L. C. Bassett, Near-infrared-assisted charge control and spin readout of the nitrogen-vacancy center in diamond, Phys. Rev. B **94**, 241201(R) (2016).
[14] J. M. Boss, K. S. Cujia, J. Zopes, and C. L. Degen, Quantum sensing with arbitrary frequency resolution, Science **356**, 837 (2017).
[15] S. Schmitt, T. Gefen, F. M. Stürner, T. Unden, G. Wolff, C. Müller, J. Scheuer, B. Naydenov, M. Markham, S. Pezzagna, J. Meijer, I. Schwarz, M. Plenio, A. Retzker, L. P. McGuinness, and F. Jelezko, Submillihertz magnetic spectroscopy performed with a nanoscale quantum sensor, Science **356**, 832 (2017).
[16] D. R. Glenn, D. B. Bucher, J. Lee, M. D. Lukin, H. Park, and R. L. Walsworth, High-resolution magnetic resonance spectroscopy using a solid-state spin sensor, Nature **555**, 351 (2018).
[17] L. Robledo, H. Bernien, T. van der Sar, and R. Hanson, Spin dynamics in the optical cycle of single nitrogen-vacancy centres in diamond, New J. Phys. **13**, 025013 (2011).
[18] G. Balasubramanian, P. Neumann, D. Twitchen, M. Markham, R. Kolesov, N. Mizuochi, J. Isoya, J. Achard, J. Beck, J. Tissler, V. Jacques, P. R. Hemmer, F. Jelezko, and J. Wrachtrup, Ultralong spin coherence time in isotopically engineered diamond, Nat. Mater. **8**, 383 (2009).
[19] S. Steinert, F. Dolde, P. Neumann, A. Aird, B. Naydenov, G. Balasubramanian, F. Jelezko, and J. Wrachtrup, High sensitivity magnetic imaging using an array of spins in diamond, Rev. Sci. Instrum. **81**, 043705 (2010).
[20] L. M. Pham, D. Le Sage, P. L. Stanwix, T. K. Yeung, D. Glenn, A. Trifonov, P. Cappellaro, P. R. Hemmer, M. D. Lukin, H. Park, A. Yacoby, and R. L. Walsworth, Magnetic field imaging with nitrogen-vacancy ensembles, New J. Phys. **13**, 045021 (2011).
[21] D. Le Sage, L. M. Pham, N. Bar-Gill, C. Belthangady, M. D. Lukin, A. Yacoby, and R. L. Walsworth, Efficient photon detection from color centers in a diamond optical waveguide, Phys. Rev. B **85**, 121202(R) (2012).
[22] D. Wildanger, B. R. Patton, H. Schill, L. Marseglia, J. P. Hadden, S. Knauer, A. Schönle, J. G. Rarity, J. L. O'Brien, S. W. Hell, and J. M. Smith, Solid immersion facilitates fluorescence microscopy with nanometer resolution and sub-ångström emitter localization, Adv. Mat. **24**, OP309 (2012).
[23] L. Li, E. H. Chen, J. Zheng, S. L. Mouradian, F. Dolde, T. Schröder, S. Karaveli, M. L. Markham, D. J. Twitchen, and D. Englund, Efficient photon collection from a nitrogen vacancy center in a circular bullseye grating, Nano Lett. **15**, 1493 (2015).
[24] M. J. Burek, N. P. de Leon, B. J. Shields, B. J. M. Hausmann, Y. Chu, Q. Quan, A. S. Zibrov, H. Park, M. D. Lukin, and M. Lončar, Free-standing mechanical and photonic nanostructures in single-crystal diamond, Nano Lett. **12**, 6084 (2012).
[25] L. Jiang, J. S. Hodges, J. R. Maze, P. Maurer, J. M. Taylor, D. G. Cory, P. R. Hemmer, R. L. Walsworth, A. Yacoby, A. S. Zibrov, and M. D. Lukin, Repetitive readout of a single electronic spin via quantum logic with nuclear spin ancillae, Science **326**, 267 (2009).
[26] M. W. Doherty, N. B. Manson, P. Delaney, F. Jelezko, J. Wrachtrup, and L. C. L. Hollenberg, The nitrogen-vacancy colour centre in diamond, Phys. Rep. **528**, 1 (2013).
[27] K. Y. Han, S. K. Kim, C. Eggeling, and S. W. Hell, Metastable dark states enable ground state depletion microscopy of nitrogen vacancy centers in diamond with diffraction-unlimited resolution, Nano Lett. **10**, 3199 (2010).
[28] G. Waldherr, J. Beck, M. Steiner, P. Neumann, A. Gali, T. Frauenheim, F. Jelezko, and J. Wrachtrup, Dark states of single nitrogen-vacancy centers in diamond unraveled by single shot NMR, Phys. Rev. Lett. **106**, 157601 (2011).
[29] K. Beha, A. Batalov, N. B. Manson, R. Bratschitsch, and A. Leitenstorfer, Optimum photoluminescence excitation and recharging cycle of single nitrogen-vacancy centers in

ultrapure diamond, Phys. Rev. Lett. **109**, 097404 (2012).
[30] N. Aslam, G. Waldherr, P. Neumann, F. Jelezko, and J. Wrachtrup, Photo-induced ionization dynamics of the nitrogen vacancy defect in diamond investigated by single-shot charge state detection, New J. Phys. **15**, 013064 (2013).
[31] G. de Lange, Z. H. Wang, D. Ristè, V. V. Dobrovitski, and R. Hanson, Universal dynamical decoupling of a single solid-state spin from a spin bath, Science **330**, 60 (2010).
[32] L. M. Pham, N. Bar-Gill, C. Belthangady, D. Le Sage, P. Cappellaro, M. D. Lukin, A. Yacoby, and R. L. Walsworth, Enhanced solid-state multispin metrology using dynamical decoupling, Phys. Rev. B **86**, 045214 (2012).
[33] G. Balasubramanian, I. Y. Chan, R. Kolesov, M. Al-Hmoud, J. Tisler, C. Shin, C. Kim, A. Wojcik, P. R. Hemmer, A. Krueger, T. Hanke, A. Leitenstorfer, R. Bratschitsch, F. Jelezko, and J. Wrachtrup, Nanoscale imaging magnetometry with diamond spins under ambient conditions, Nature **455**, 648 (2008).
[34] J. R. Maze, P. L. Stanwix, J. S. Hodges, S. Hong, J. M. Taylor, P. Cappellaro, L. Jiang, M. V. G. Dutt, E. Togan, A. S. Zibrov, A. Yacoby, R. L. Walsworth, and M. D. Lukin, Nanoscale magnetic sensing with an individual electronic spin in diamond, Nature **455**, 644 (2008).
[35] N. Bar-Gill, L. M. Pham, A. Jarmola, D. Budker, and R. L. Walsworth, Solid-state electronic spin coherence time approaching one second, Nat. Commun. **4**, 1743 (2013).
[36] G. Kucsko, P. C. Maurer, N. Y. Yao, M. Kubo, H. J. Noh, P. K. Lo, H. Park, and M. D. Lukin, Nanometre-scale thermometry in a living cell, Nature **500**, 54 (2013).
[37] A. Ajoy, Y. X. Liu, and P. Cappellaro, DC magnetometry at the T_2 limit, arXiv:1611.04691 (2016).
[38] C. Bonato, M. S. Blok, H. T. Dinani, D. W. Berry, M. L. Markham, D. J. Twitchen, and R. Hanson, Optimized quantum sensing with a single electron spin using real-time adaptive measurements, Nat. Nanotech. **11**, 247 (2016).
[39] A. Ariyaratne, D. Bluvstein, B. A. Myers, and A. C. B. Jayich, Nanoscale electrical conductivity imaging using a nitrogen-vacancy center in diamond, Nat. Commun. **9**, 2406 (2018).
[40] D. A. Hopper, R. R. Grote, S. M. Parks, and L. C. Bassett, Amplified sensitivity of nitrogen-vacancy spins in nanodiamonds using all-optical charge readout, ACS Nano **12**, 4678 (2018).
[41] H. Jayakumar, S. Dhomkar, J. Henshaw, and C. A. Meriles, Spin readout via spin-to-charge conversion in bulk diamond nitrogen-vacancy ensembles, Appl. Phys. Lett. **113**, 122404 (2018).
[42] P. C. Maurer, J. R. Maze, P. L. Stanwix, L. Jiang, A. V. Gorshkov, A. A. Zibrov, B. Harke, J. S. Hodges, A. S. Zibrov, A. Yacoby, D. Twitchen, S. W. Hell, R. L. Walsworth, and M. D. Lukin, Far-field optical imaging and manipulation of individual spins with nanoscale resolution, Nat. Phys. **6**, 912 (2010).
[43] J.-C. Jaskula, E. Bauch, S. Arroyo-Camejo, M. D. Lukin, S. W. Hell, A. S. Trifonov, and R. L. Walsworth, Super-resolution optical magnetic imaging and spectroscopy using individual electronic spins in diamond, Opt. Express **25**, 11048 (2017).
[44] A. O. Sushkov, N. Chisholm, I. Lovchinsky, M. Kubo, P. K. Lo, S. D. Bennett, D. Hunger, A. Akimov, R. L. Walsworth, H. Park, and M. D. Lukin, All-optical sensing of a single-molecule electron spin, Nano Lett. **14**, 6443 (2014).
[45] T. Staudacher, F. Shi, S. Pezzagna, J. Meijer, J. Du, C. A. Meriles, F. Reinhard, and J. Wrachtrup, Nuclear magnetic resonance spectroscopy on a (5-nanometer)3 sample volume, Science **339**, 561 (2013).
[46] H. J. Mamin, M. Kim, M. H. Sherwood, C. T. Rettner, K. Ohno, D. D. Awschalom, and D. Rugar, Nanoscale nuclear magnetic resonance with a nitrogen-vacancy spin sensor, Science **339**, 557 (2013).
[47] L. M. Pham, S. J. DeVience, F. Casola, I. Lovchinsky, A. O. Sushkov, E. Bersin, J. Lee, E. Urbach, P. Cappellaro, H. Park, A. Yacoby, M. Lukin, and R. L. Walsworth, NMR technique for determining the depth of shallow nitrogen-vacancy centers in diamond, Phys. Rev. B **93**, 045425 (2016).